Received 10 December 2022; revised 10 June 2023; accepted 23 June 2023. Date of publication 30 June 2023; date of current version 5 July 2023.

*Digital Object Identifier 10.1109/OJAP.2023.3290981*

# Statistical Evaluation of the Role of GNSS Signal Propagation Orientation in Low-Latitude Amplitude Scintillation Severity

**ALISON MORAES[1], JONAS SOUSASANTOS[2], BRUNO J. AFFONSO[3], PAULO R. P. SILVA[3], EURICO R. DE PAULA[4], AND JOÃO F. G. MONICO[5]**

[1]Divisão de Eletrônica, Instituto de Aeronáutica e Espaço, São José dos Campos 12284465, Brazil

[2]William B. Hanson Center for Space Sciences, University of Texas at Dallas, Richardson, TX 75080, USA

[3]Programa de Pós Graduação em Engenharia Eletrônica e de Computação, Instituto Tecnológico de Aeronáutica, São José dos Campos 12228-900, Brazil

[4]Divisão de Heliofísica, Ciências Planetárias e Aeronomia, Instituto Nacional de Pesquisas Espaciais, São José dos Campos 12227-010, Brazil

[5]Departamento de Cartografia, Universidade Estadual Paulista Júlio de Mesquita Filho, São José dos Campos 12224-300, Brazil

CORRESPONDING AUTHOR: A. MORAES (e-mail: aom@ita.br)

This work was supported by the framework of INCT GNSS-NavAer Project under Grant CNPq 465648/2014-2 and Grant FAPESP 2017/50115-0. The work of Alison Moraes was supported by the Conselho Nacional de Desenvolvimento Científico e Tecnológico (CNPq) under Grant 309389/2021-6. The work of Jonas Sousasantos was supported by NSF under Award AGS-1916055 and Award FAPESP 2018/06158-9. The work of Paulo R. P. Silva was supported by CAPES under Grant 88887.373639/2019. The work of Eurico R. De Paula was supported by CNPq under Grant 202531/2019-0. The work of JOÃO F. G. Monico was supported by CNPq under Grant 304773/2021-2.

**ABSTRACT** Equatorial plasma bubbles are depleted plasma structures aligned to the geomagnetic field lines that are generated in the nighttime ionosphere bottomside and rise to the topside extending to increasingly higher latitudes. These structures induce fluctuations in the transionospheric radio signals causing the phenomenon known as ionospheric scintillation. Ionospheric scintillation is one of the main concerns for safety critical applications that rely on Global Navigation Satellite System information, therefore, the understanding about the occurrence and severity of scintillation is necessary. In this work, an analysis considering aspects of the orientation of the propagation of the radio signals through the plasma bubbles structures is performed to evaluate how this geometry can affect the scintillation profile. The dataset covers five months of records from three stations over the Brazilian region during the last solar cycle maximum. The initial results indicate that propagation paths fully aligned are consistently related to larger values of $S_4$ and more severe scintillation. The statistical evaluations with the $\alpha$-$\mu$ model show that during such cases stronger fading events are expected. According to the field measurements, fading events deeper than $-15$ dB are 73% more likely to occur under some aligned environments when compared to other propagation paths.

**INDEX TERMS** Alpha-mu distribution, equatorial plasma bubbles, fading coefficients, GNSS propagation orientation.

## I. INTRODUCTION

OVER low-latitude regions, Global Navigation Satellite System (GNSS) signals may be seriously affected by ionospheric plasma irregularities. These irregularities are often manifested as severe depletions being caused by the Rayleigh-Taylor instability [1] and are known as Equatorial Plasma Bubbles (EPBs). The degradation on the radio signals caused by the EPBs occurs because these depleted structures cause variations in the amplitude and phase of the radio signals crossing their domain, this phenomenon is called ionospheric scintillation [2], [3]. The EPBs are field aligned, therefore, as the EPBs reach larger altitudes over

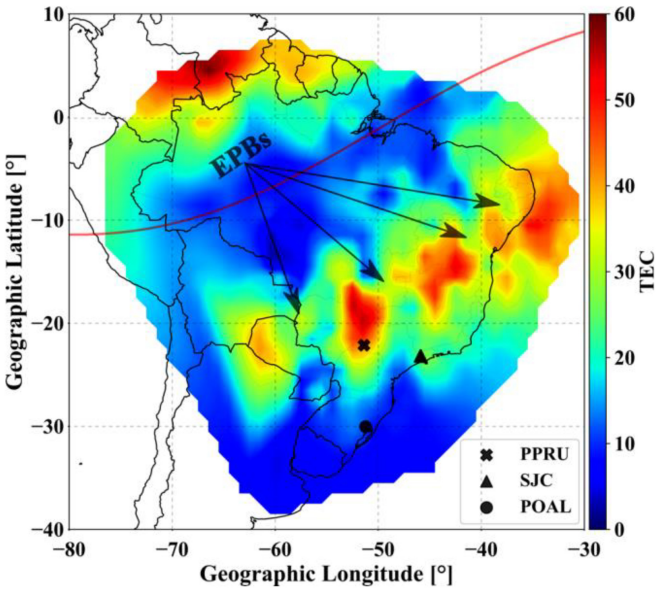


**FIGURE 1.** Example of TEC map for the night of 12/12/2014 showing the occurrence of EPBs (depleted streaks) at (00h20UT). The ground stations of Presidente Prudente (PPRU), São José dos Campos (SJC), and Porto Alegre (POAL) are also depicted.

the geomagnetic equator, they also propagate to increasingly higher latitudes [4]. The interferences of EPBs in transionospheric signals are more intense over the Equatorial Ionization Anomaly (EIA) region. In the EIA region, due to the enhanced electron density, the depleted EPBs cause a large density fluctuation, and, consequently, a more severe scintillation [5].

Fig. 1 shows the Total Electron Content (TEC) map over the Brazilian region for the night of 12/12/2014 at 00h20UT, this map was constructed according to the Marini-Pereira et al. methodology [40]. The locations of three ground stations to be used in this work are also depicted by symbols in this figure. The TEC is a quantity that measures the integrated number of electrons over the GNSS ray path considering a cylinder with unit area. Each TEC unity is equivalent to $10^{16}$ electrons/m$^2$. The TEC is assumed to be concentrated at an altitude of 350 km. This altitude is known as Ionospheric Pierce Point (IPP). In Fig. 1, the TEC values are represented by colors according to the color bar at the right. The regions of larger TEC (EIA) are clearly noticed around the geomagnetic equator (red solid line). Depleted structures indicated by the arrows may be observed across the EIA region, these are EPBs. Please notice that the EPBs cause larger TEC fluctuation (difference between EPBs and ionospheric background electron densities) over the EIA region, therefore, stronger ionospheric scintillation is expected over this region, as mentioned earlier.

Several GNSS users are affected by this type of ionospheric phenomenon and critical applications are restricted due to this obstacle. Aviation applications, for instance, have problems operating augmentation systems over low-latitude regions [6], [7]. To enhance the advancement of strategies for operating critical systems in low-latitude regions, an understanding of the ionospheric environment is essential. The theory of scintillation, which encompasses its causes and effects, serves as a well-established foundation for such studies. This is evident in previous works, including those referenced as [3] and [8], which investigate the propagation of transionospheric radio signals along the geomagnetic field lines and the associated irregularities. Characterizing the behavior of the ionosphere remains an active area of experimental research, particularly in the Brazilian sector. The spatiotemporal dynamics of Total Electron Content (TEC) and various aspects of ionospheric scintillation have been carefully investigated, considering factors such as seasonality, location, time, and solar flux, as documented in [9], [10], [11], [12], [13], [14], [15].

The unambiguous estimation of the positioning for navigation purposes depends on the availability of at least 4 satellites. Very often these signals are transmitted by satellites on distinct regions and penetrate the IPPs with distinct azimuth and elevation angles. During EPB events, this difference in the orientation of the signals implies distinct electron density fluctuation for each signal.

Previously, [8], [16], [17], [18], [19] and [20] addressed aspects related to the influence of GNSS angles of propagation, particularly elevation, and how the paths relate to the occurrence of scintillation. The study conducted by [21] revealed an enhancement of scintillation at low elevations, referred to as the end-on condition, due to the presence of field-aligned plasma bubbles. Additionally, [22] demonstrated that such enhanced scintillation is accompanied by significant variations in Ionospheric Spatial Gradients (ISGs), which represent the dynamics of Total Electron Content (TEC). These variations can potentially impact augmentation systems. Moreover, [23] demonstrated that this particular alignment between propagation orientation and EPBs leads to a notable increase in phase fluctuations, as indicated by the $\sigma_\phi$ index values. Building upon this, [24] explored how the GNSS signal propagation condition affects positioning, particularly due to a rise in cycle slip occurrences. Furthermore, [25] investigated the impact of this alignment condition on the fading profile, resulting in a higher frequency of pronounced fading events when the alignment is favorable. This work presents an analysis of the effects of GNSS signal propagation orientation in relation to the EPBs. More specifically, the goal is to understand how the statistics of scintillating signals may vary according to the propagation orientation of the signal. The statistical analyses employ the $\alpha$-$\mu$ fading model [26], [27].

In the next section, a definition of the propagation orientation between the GPS signal and the EPB is discussed. The subsequent section introduces the information about the instruments and methods to be used. In the sequence the scintillation rates according to the propagation orientation are evaluated. The following section presents the $\alpha$-$\mu$ model and a discussion on how the scintillation profile changes as a function of the signal propagation orientation. The conclusion presents a summary of the main findings on the role of GNSS signal propagation on scintillation probability and statistics.

## II. DEFINITION OF PROPAGATION ORIENTATION

Before introducing the instrumentation and methods, it is first necessary to discuss the definitions of propagation orientation that will be used in the next sections. There are three possible configurations that are considered, fully aligned, partially aligned and nonaligned. The fully aligned condition corresponds to the cases when the length of the radio signal propagation path through the EPBs is maximized. As mentioned earlier, EPBs are geomagnetic field aligned structures, hence, a transionospheric signal may be considered fully aligned to the EPBs if, at the IPP altitude, its orientation coincides with the direction of the geomagnetic field lines. This congruence may be evaluated by comparing the satellite elevation angle with the geomagnetic inclination, and the satellite azimuth angle with the geomagnetic declination, both at the IPP altitude.

The nonaligned condition corresponds to the cases when the signal intercepts the EPBs, but the length of the propagation path through the EPBs is minimized because it is more perpendicular to the direction of the EPB structure. The partially alignment conditions correspond to cases when the propagation path presents either an alignment between the GNSS azimuth and the geomagnetic field declination or between the GNSS elevation and the geomagnetic field inclination, but not both at the same time.

To compare these angles, and perform the classification, the first step is to calculate the IPP geographic coordinates for each observation. To do so the ionosphere is assumed as a thin shell at the IPP altitude (350 km). In the sequence, the geomagnetic inclination and declination were calculated for each IPP. The geomagnetic field inclination and declination angles are derived from the International Geomagnetic Reference Field (IGRF-12) [28].

The difference between the GNSS elevation angles and the geomagnetic field inclination at each IPP is represented by the parameter $\omega$. The difference between the GNSS azimuth angles and the geomagnetic declination at each IPP is represented by the parameter $\nu$. These two angular parameters are calculated according to the definition of [24]. In this work, it was assumed that the fully aligned condition was achieved if both, $|\omega|$ and $|\nu|$, are simultaneously less than or equal to 15°. When $|\omega|$ and $|\nu|$ are both greater than 15°, the signal was classified as nonaligned. The cases when only one parameter, $|\omega|$ or $|\nu|$, is less than or equal to 15°, were classified as partially aligned.

To illustrate these angles, Fig. 2 presents the geometry involved in the calculation of the parameters $\omega$ and $\nu$. Only one station was considered in the figure to avoid too many graphical elements. The station considered was Presidente Prudente and its respective IPP location is described by a black circle at 350 km. The red solid line describes the geomagnetic field line whose IPP at 350 km is over Presidente Prudente. The dashed red lines correspond to the directions of the geomagnetic field line at the IPP altitude. The color-coded contour is the same used in Fig. 1, and represents the TEC distribution, at the IPP altitude, over the

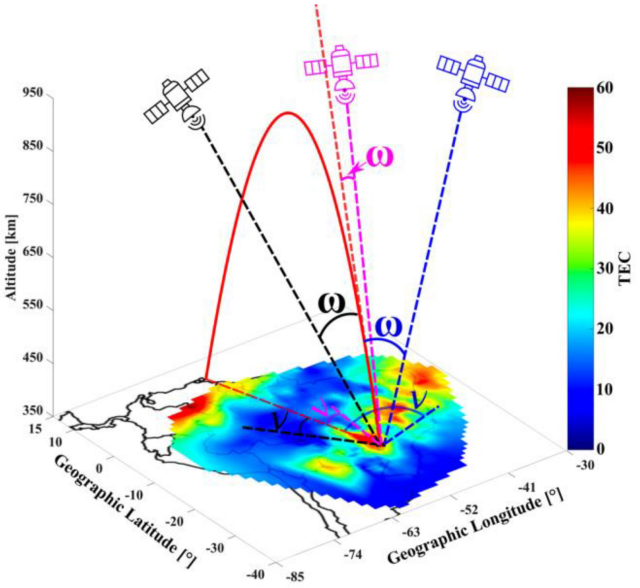


**FIGURE 2.** Graphic representation of the geometry involved in the calculation of the $\omega$ and $\nu$ angles. The red solid line represents the geomagnetic field line passing over Presidente Prudente (black circle) at the IPP altitude. The red dashed lines describe the directions of the geomagnetic field line at the IPP altitude. The black, magenta, and blue lines describe hypothetic ray paths from three GNSS satellites. The color-coded contour shows the TEC over the Brazilian region. As one can notice, some signals are more aligned with the geomagnetic field lines than others.

Brazilian region. The black, magenta, and blue dashed lines correspond to hypothetical ray paths from three GNSS satellites recorded by the station considered. The angles between each GNSS elevation and the geomagnetic field inclination are described by $\omega$ using the same color of the signal transmitted. Similarly, the angles between each GNSS azimuth and the geomagnetic field declination are described by $\nu$ using the same color of the signal transmitted, but this time it must be observed that the $\nu$ angles reside in the latitude $\times$ longitude plane. As can be readily seen, some signals are more aligned with the geomagnetic field line than others, and since EPBs are field aligned, these signals will be more aligned to the EPBs as well. As an example, the signal represented by the magenta color has a similar $\nu$ angle when compared to the signal depicted in black, however, the $\omega$ angle for the signal in magenta is much smaller. Consequently, the signal in magenta would be "fully aligned", while the signal in black would be classified as "partially aligned". According to the aforementioned definitions, the signal in blue would be classified as "nonaligned".

## III. INSTRUMENTATION AND METHODS

The scintillation records used in this investigation were acquired by three ground stations located in the Brazilian southern sector. The locations of these stations were already depicted in Fig. 1 and 2. More specific details about the stations used are provided in Table 1. The three stations that acquired the data belong to the INCT NavAer network [29] and were equipped with Septentrio PolaRxS

**TABLE 1.** Location of analyzed stations.

| | Presidente Prudente (PPRU) | São José dos Campos (SJC) | Porto Alegre (POAL) |
|---|---|---|---|
| Latitude | -22.12° | -23.20° | -30.07° |
| Longitude | -51.40° | -45.85° | -51.11° |
| Dip angle | -16.01° | -19.28° | -22.32° |

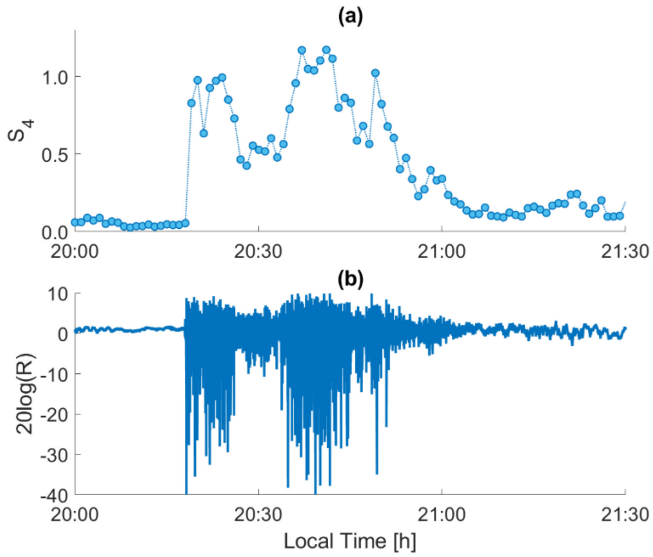


**FIGURE 3.** One example of a signal affected by EPBs causing scintillation during 11/13/2014. This signal was transmitted by the PRN 25 and recorded by the SJC station. Panel (a): estimated amplitude scintillation index $S_4$. Panel (b): Detrended signal intensity.

scintillation monitors. The period of investigation covers the nights from 11/01/2014 up to 03/30/2015. The hours of observation at each night range from 19:00 LT up to 23:59 LT. The analyzed signals were the Global Positioning System (GPS) L1 records (1575.42 MHz), and the amplitude scintillation data had a sampling rate of 50 Hz. More details on data processing for this and for other scintillation monitors can be found in [30]. The data were classified according to the amplitude scintillation index $S_4$, given by [3]

$$S_4 = \sqrt{\frac{\langle I^2 \rangle - \langle I \rangle^2}{\langle I \rangle^2}}, \tag{1}$$

where $I=R^2$ is the intensity of the received signal with amplitude R. This index is computed with a 3000 samples vector, referring to the period of one minute [15].

Fig. 3 presents one example of the signal suffering scintillation. Panel (a) shows the estimated $S_4$, and panel (b) exhibits the detrended signal intensity for the night of 11/13/2014. This signal was transmitted by the PRN 25 and recorded by the São José dos Campos ground station. Note that, as the strength of the scintillation increases, with more serious fading events, the higher the $S_4$ becomes.

## IV. ON THE RATE OF SCINTILLATION ACCORDING TO THE PROPAGATION ORIENTATION

Critical systems rely on navigation information complying with strict availability and integrity standards, therefore, information about the probability of scintillation on the signals used for these applications is helpful. Reference [7], for example, presented a case when the Ground-Based Augmentation System (GBAS) suffered degradation due the occurrence of scintillation over the southern Brazilian region. Reference [14] presented probabilities of scintillation occurrences for the stations of Presidente Prudente, São José dos Campos and Porto Alegre. In their work, the authors did not consider the influence of the orientation of signal propagation in the results. Also, [14] observed that, for $S_4 > 0.3$, the probabilities of scintillation occurrence were increasingly higher over Porto Alegre, São José dos Campos and Presidente Prudente, respectively. This result is presumably related to the fact that as stations whose IPPs are more concentric with the peak of the EIA are considered, the more affected the signals are expected to be. But it might be that other factors, such as the signal propagation path, are also contributing, as shall be discussed ahead.

Fig. 4 shows Complementary Cumulative Distribution Function (CCDF) curves for the stations of Presidente Prudente (panel a), São José dos Campos (panel b), and Porto Alegre (panel c). Each curve corresponds to a distinct propagation path configuration. The results consider propagation paths that are fully aligned (solid blue line), nonaligned (solid orange line), partially aligned with only $|\nu| < 15°$ (solid yellow line), and partially aligned with only $|\omega| < 15°$ (solid purple line). An additional general curve (dashed green line) considering all the measurements is also presented.

The fully aligned propagation path has the largest probabilities for more severe scintillation cases, i.e., larger values of $S_4$ for all the stations. For the aligned case, the CCDF curves show an abrupt change from 0.3 to 0.7. The second largest probabilities during strong scintillation are those from cases under partial alignment in elevation ($|\omega| < 15°$). Despite being the second most affected condition, the values are considerably smaller than those from the aligned cases. For example, taking the case where $S_4 > 0.8$ in São José dos Campos, the probabilities are 15.9% and 5.6%, respectively, for fully aligned and partially aligned in elevation. In this case, there are approximately 3 times more chances of being affected by scintillation under the fully aligned condition.

In Fig. 4, the cases under partial alignment in azimuth ($|\nu| < 15°$) and nonaligned cases presented the smallest probabilities, with much reduced CCDF curves, even smaller than the general CCDF curves. Comparing these two less susceptible conditions to scintillation with the aligned condition, one can note that the differences in the probabilities may reach up to ∼10 times when considering levels of strong scintillation. As an example, considering again $S_4 > 0.8$ in São José dos Campos, the probabilities are 0.81%, 1.35%, 5.64%, and

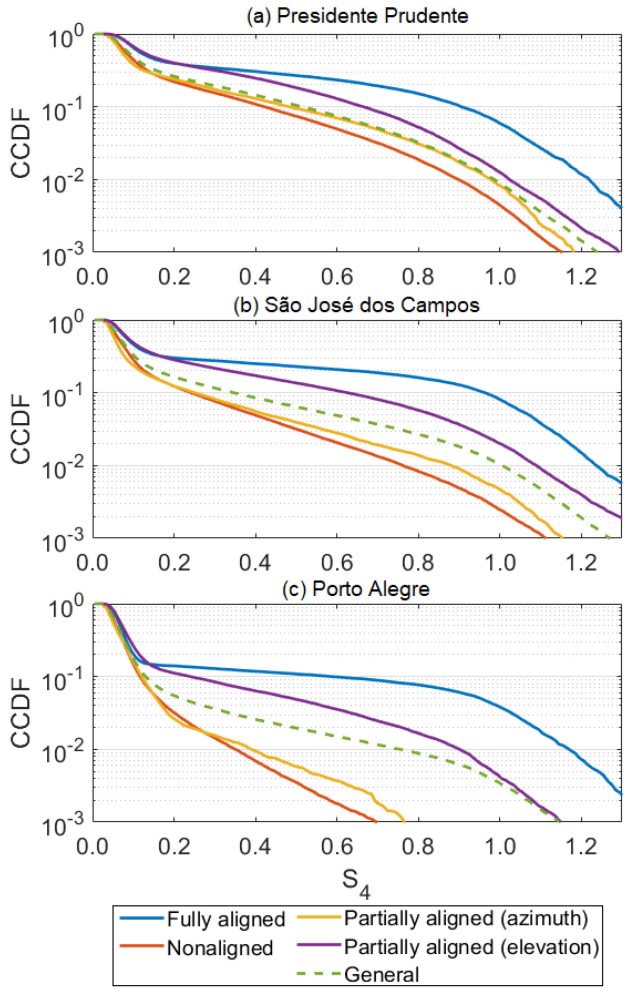


**FIGURE 4.** Complementary Cumulative Distribution Functions (CCDF) of $S_4$ for GPS L1 signals under different propagation conditions considering stations of Presidente Prudente (a), São José dos Campos (b) and Porto Alegre (c).

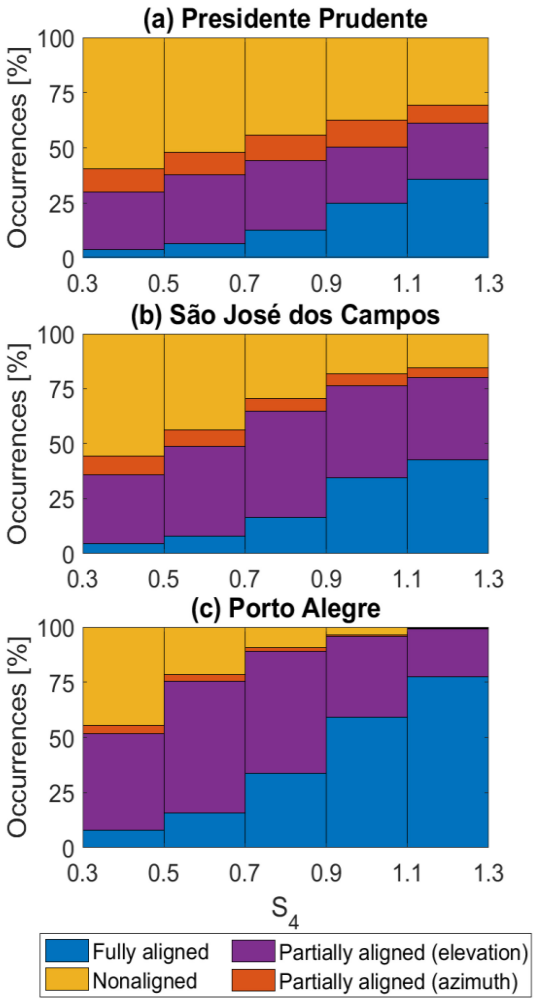


**FIGURE 5.** Percentage of fully aligned, partially aligned and nonaligned cases for different $S_4$ levels.

15.99%, for nonaligned, partially azimuth-aligned, partially elevation-aligned, and fully aligned, respectively.

It is worth mentioning that for all the evaluated conditions the relationship observed by [14] is valid, that is, Presidente Prudente is the station with the largest values in the CCDF when compared to the other stations, and Porto Alegre is the stations with the smallest probabilities of occurrence.

Fig. 5 shows the proportionalities of each alignment condition for each $S_4$ level considered. Please note that for all $S_4$ levels, the summation of the contribution from the four conditions reaches 100%, i.e., it corresponds to the total cases for this level of $S_4$ in the dataset considered. On the one hand, it is possible to verify that as $S_4$ increases, the participation of nonaligned cases decreases for the three stations considered. On the other hand, the increase in $S_4$ seems to be directly related to the growth of the fully aligned cases. The cases that are partially aligned in elevation also follow the trend of the fully aligned, however, cases that are partially aligned only in azimuth are not very expressive. The cases that are partially aligned in azimuth also correspond to an approximately constant portion of the cases for all the levels of $S_4$, not showing any increasing trend.

When comparing the stations, there are also differences that can be highlighted. The number of fully aligned cases is more relevant as more southward stations are considered. Presidente Prudente is below the EIA (see Fig. 1), this location ends up having more non-aligned cases. However, São José dos Campos and Porto Alegre have part of their sky view at the IPP altitudes outside the EIA. This configuration, surprisingly, minimizes the nonalignment, increasing the rate of occurrence of aligned cases. For example, the nonaligned cases in the range $0.5 < S_4 \leq 0.7$ were 53.0%, 43.3%, and 21.5% for Presidente Prudente, São José dos Campos, and Porto Alegre, respectively. For fully aligned cases in the range $0.9 < S_4 \leq 1.1$, the numbers were 24.7%, 34.5%, and 59.2% for Presidente Prudente, São José dos Campos, and Porto Alegre, respectively.

According to these results, there are two aspects to be considered, the first is that locations below the EIA, like Presidente Prudente, are likely to have more nonaligned cases, but these cases typically have lower $S_4$ values. The

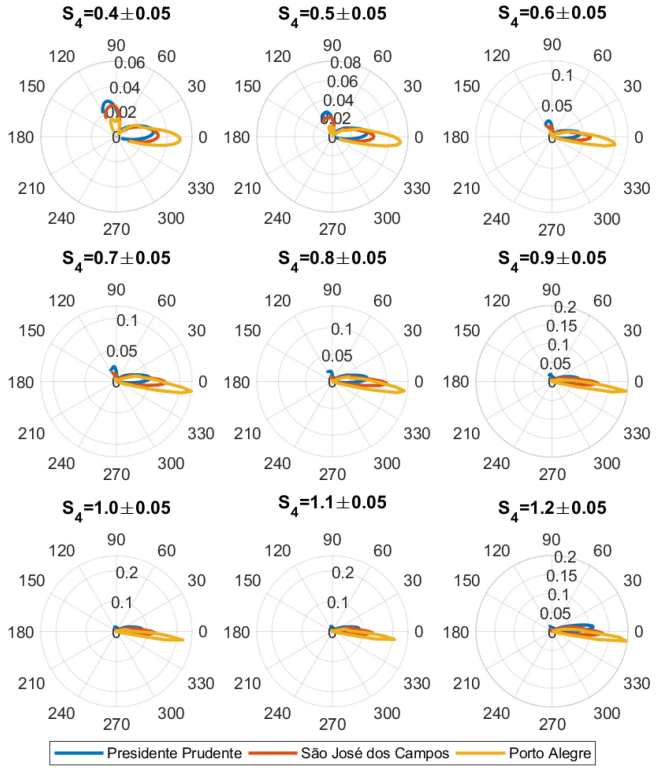


**FIGURE 6.** Probability density function of scintillation occurrences according to $\omega$.

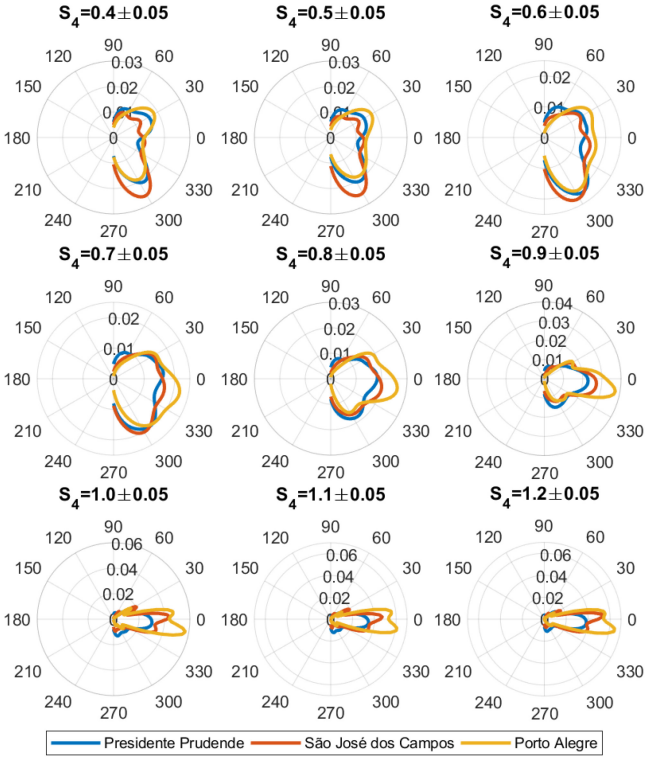


**FIGURE 7.** Probability density function of scintillation occurrences as a function of $\nu$.

second is that locations in the boundary of the EIA, like São José dos Campos and Porto Alegre, do not have many nonaligned cases, i.e., these stations have less occurrence of scintillation, however, when these stations experience scintillation, since the signals are more likely to be aligned, the severity of the scintillation will be stronger. Therefore, the role of the alignment condition is considerable.

To investigate in further detail the influence of the geomagnetic field orientation along the GNSS signal path the scintillation cases will now be decomposed according to the angles $\omega$ and $\nu$. Fig. 6 shows estimated probability densities of scintillation occurrences according to $\omega$. Each panel corresponds to a given $S_4$ level and shows its empirical probability distribution according to the angle $\omega$ in the range $-20° \leq \omega \leq 120°$. The levels of $S_4$ considered $0.4 \pm 0.05 \leq S_4 \leq 1.2 \pm 0.05$.

The results from Fig. 6 indicate two regions of concentration. The first and more prominent is around 0o, corresponding to the cases of propagation path elevation aligned to the geomagnetic inclination. For $S_4 > 0.7$ these aligned cases become the absolute empirical probability environment. The second region of concentration of probability resides $90° \leq \omega \leq 120°$, corresponding to the cases close to the zenith. Another aspect worth mentioning is that the second region is almost nonexistent in Porto Alegre due to its location and slightly larger for São José dos Campos (but smaller than Presidente Prudente).

Fig. 7 is analogous to Fig. 6, but in that case the probability densities were estimated according to the parameter $\nu$ in the range $-90° \leq \nu \leq 90°$. The results presented in the panels of Fig. 7 agree with those presented in Fig. 5 for $S_4 \leq 0.7$, i.e., the scintillations with low and moderate strength have small contributions from the azimuthal alignment condition. For these $S_4$ levels, it is observed that the scintillation cases (represented through the estimated probability densities) are spread. For levels of $S_4 \geq 0.9$, the scintillation events tend to converge to lower values of $|\nu|$. In fact, cases of extreme scintillation levels ($S_4 \geq 1.0$) are concentrated almost exclusively around very small values of $|\nu|$.

A combined analysis of the results presented in Fig. 6 and 7 indicates that the occurrence of scintillation over all the scintillation levels seems to be directly related to the orientation of the propagation path across the geomagnetic field lines around the IPP altitude. The results suggest that cases partially aligned in elevation seem to be more critical, however, cases of strong and extreme scintillation ($S_4 > 0.8$) are more likely to occur under fully aligned conditions. More specifically, cases of $S_4 < 0.8$ apparently may be generated under any azimuth orientation, while cases of stronger scintillation are favored during fully alignment conditions. These results agree with those previously reported by [24].

It must be highlighted that Presidente Prudente, although experiencing less alignment, has more scintillation events, as shown in Fig. 4. Over the other stations located around the boundaries of the EIA the alignment favorable condition has a greater role.

## V. $\alpha$-$\mu$ FADING MODELING

In the existing literature, numerous models have been employed to fit scintillation data, including Nakagami-*m* [31] and Rice [32]. Notably, [33] and [34] utilized the $\alpha$-$\mu$ model [26] to characterize scintillation statistics, and their findings displayed a remarkable resemblance to field data. An illustrative example is the study conducted by [9], which revealed that the frequency of scintillation events varies with the solar cycle period, while the typical values of the $\alpha$-$\mu$ model remain stable regardless of the cycle phase. In other words, the solar cycle serves as the primary driver of the occurrence and intensity of scintillation, but the statistical properties of scintillation events typically adhere to a consistent behavior. Given the $\alpha$-$\mu$ model's ability to realistically represent scintillation, simulation models of scintillation have also adopted this distribution in their experiments [35], [36].

Considering a normalized signal, $E(R^2)=1$, the probability density function (PDF) of the $\alpha$-$\mu$ distribution will be given by [33]

$$f_R(r) = \left[\frac{\alpha r^{\alpha\mu-1}}{\xi^{\alpha\mu/2}\Gamma(\mu)}\right] e^{\left(\frac{-r^{\alpha}}{\xi^{\alpha/2}}\right)}, \tag{2}$$

where r is the received signal amplitude, $\Gamma$ is the Gamma function, and $\xi = \Gamma(\mu)/\Gamma(\mu + 2/\alpha)$.

The Cumulative Distribution Function (CDF), $F_R(r)$, for the $\alpha$-$\mu$ model, considering $E(R^2)=1$, is expressed by [26]

$$F_R(r) = \frac{\Gamma\left[\mu, \left(r/\sqrt{\xi}\right)^{\alpha}\right]}{\Gamma(\mu)}, \tag{3}$$

where, for two functions $\varphi$ and $\psi$, $\Gamma[\varphi, \psi] = \int_0^{\psi} t^{(\varphi-1)} e^{-t} dt$ is the incomplete Gamma function. As one can note, the probability of a fading event smaller than a certain value of received signal amplitude, r, may be estimated using (3).

It is also convenient to relate the pair of fading coefficients $\alpha$-$\mu$ with the $S_4$ index. This relation, according to [33], may be defined by

$$S_4 = \left(\frac{\Gamma(\mu)\Gamma(\mu + 4/\alpha) - \Gamma^2(\mu + 2/\alpha)}{\Gamma^2(\mu + 2/\alpha)}\right)^{\frac{1}{2}}. \tag{4}$$

There are, of course, infinite pairs of $\alpha$ and $\mu$ that satisfy (4); therefore, the procedure is to estimate the pair of coefficients that best describes scintillation. In the literature, there are different methods for estimating this pair. Examples include moment-based estimators [26]. In the present work, the Maximum-Likelihood Estimation (MLE) procedure was employed [37], [38]. The coefficients of (2) are adjusted to the empirical PDF at each one-minute of data recorded.

Fig. 8 exhibits one example of the ability of the $\alpha$-$\mu$ model to fit the field data. The upper panel shows a one-minute interval of a scintillating received signal ($S_4 \approx 0.9$). Applying the MLE procedure to this record, the fading coefficients $\alpha$ and $\mu$ were estimated as 1.07 and 4.57, respectively. The lower panel displays the Cumulative Distribution Function of (3), $F_R(r)$, for the estimated $\alpha$-$\mu$ pair (blue line) together with the empirical CDF (cyan circles). This panel also shows

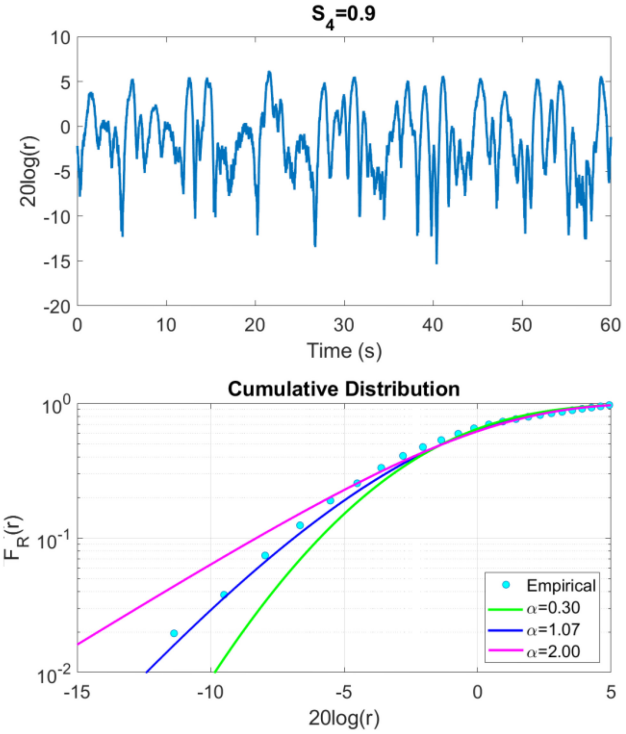


**FIGURE 8.** Upper panel: Example of a received signal suffering scintillation ($S_4 \approx 0.9$). Lower panel: Empirical (cyan dots) and theoretical Cumulative Distribution Functions (solid lines) for three different values of $\alpha$ considering the values shown in the lower right panel. When $\alpha = 1.07$ is considered, the model adjustment presents good agreement with the empirical data.

other two cases of (3), for $\alpha = 2.00$ with $\mu = 1.22$ (magenta line), and for $\alpha = 0.30$ with $\mu = 68.52$ (green line). These extra curves were introduced to exemplify how the fading coefficients regulate the shape of the distribution, and how this model adjusts properly to real data in the "tail region". As mentioned earlier, (3) may be used to estimate how severe the scintillation may be according to the $\alpha$-$\mu$ pair. As an example, consider $F_R$ for a signal intensity of $-10$ dB in (3), in this case, the probabilities of $r^2 \leq -10$ dB are 0.8%, 2.9%, and 6.3% for $\alpha = 0.30$, 1.07, and 2.00, respectively, respectively. Therefore, $\alpha$ may be interpreted as an auxiliary parameter to the $S_4$ index, providing the statistical behavior of the fading events. Increasing values of $\alpha$ correspond to distributions with "more raised tails", indicating larger probabilities of deep fading events.

Reference [39] showed that fades deeper than $-15$ dB may cause serious receiver unavailability issues due to the high probability of cycle slips. Also, [15] showed that fades deeper than $-15$ dB are frequent under strong scintillation. Therefore, the $\alpha$-$\mu$ model might be used to indicate critical cases for users.

## VI. FADING COEFFICIENTS ACCORDING TO PROPAGATION ORIENTATION

Previously, [38] presented a general analysis about fading coefficients at the stations of Presidente Prudente, São José dos Campos, and Porto Alegre. In their work, they observed

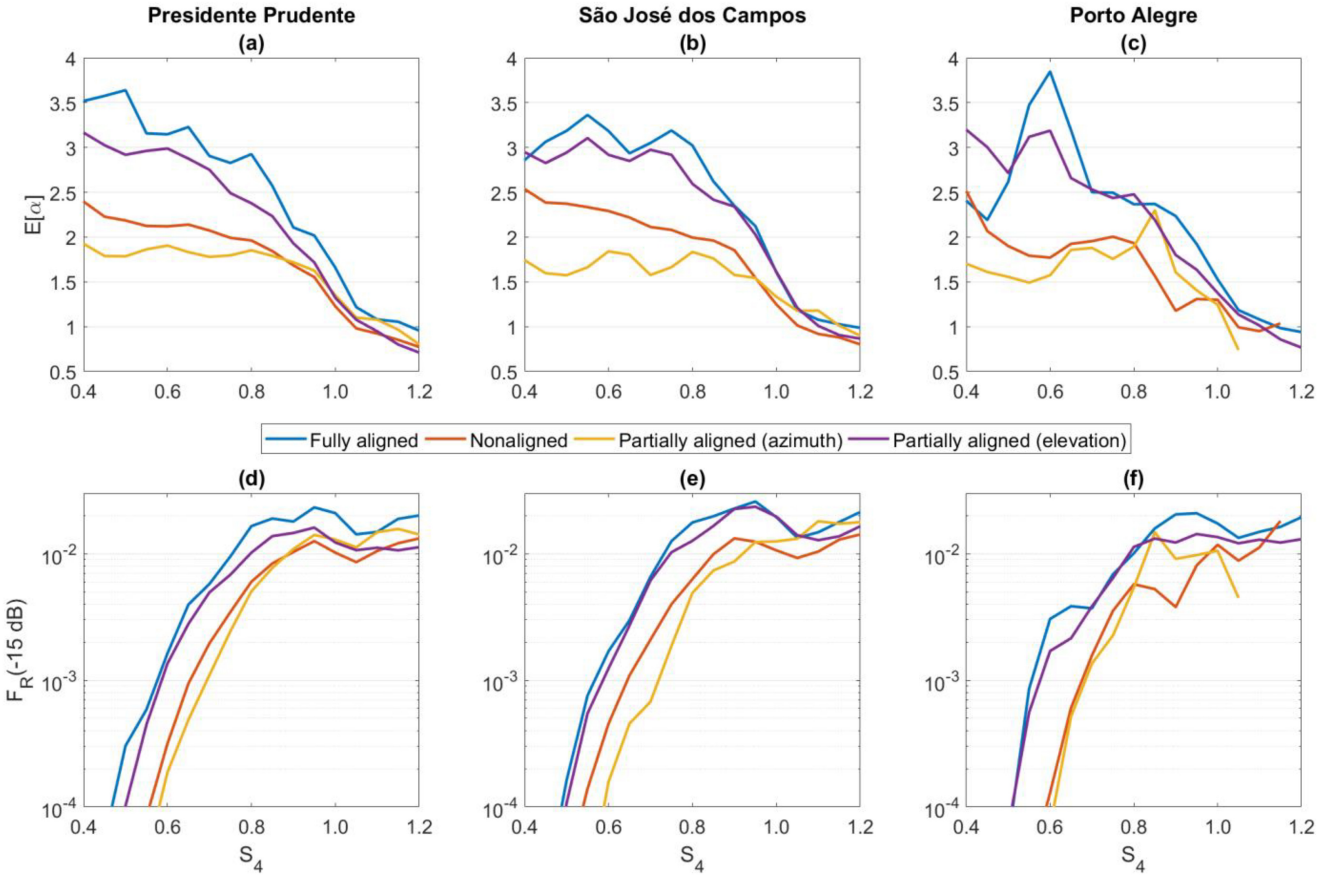


**FIGURE 9.** Upper panels: mean values of $\alpha$ according to different values of S4 for Presidente Prudente (a), São José dos Campos (b), and Porto Alegre (c) considering fully aligned (blue), partially elevation-aligned (purple), partially azimuth-aligned (yellow) and nonaligned (orange) conditions. Lower panels: estimated probability of having fading events deeper than −15 dB for Presidente Prudente (d), São José dos Campos (e), and Porto Alegre (f) considering fully aligned (blue), partially elevation-aligned (purple), partially azimuth-aligned (yellow) and nonaligned (orange) conditions.

that the largest values of $\alpha$, considering cases of $S_4 > 0.6$, occurred over São José dos Campos. Porto Alegre presented the second largest values of $\alpha$ and, surprisingly, Presidente Prudente exhibited the smallest values of $\alpha$, despite the fact of being below the EIA peak.

With the information of the proper pair of fading coefficients ($\alpha$, $\mu$) and the corresponding values of $S_4$ it is possible to characterize the statistics of fading events according to propagation orientation, hence, exploring in more details underlying aspects of these differences between stations/locations. Panels (a), (b) and (c) of Fig. 9 presents, for each station, the mean values of the estimated $\alpha$ according to the $S_4$ level. The colors distinguish the fully aligned, partially elevation-aligned, partially azimuth-aligned, and nonaligned cases. It is evident that the fully aligned cases are tightly related to larger values of E[$\alpha$] when compared to the other cases for all the stations. The partially elevation-aligned cases are those with E[$\alpha$] closest to the fully aligned cases. This result indicates that the fully aligned and partially elevation-aligned cases present a "less favorable statistic" for the same values of $S_4$, i.e., the tail of the distribution is more raised and, therefore, the probability of a more severe fading is larger. Reference [24] showed similar results for a smaller dataset only considering São José dos Campos. Even for extreme scintillation ($S_4 \geq 1.0$), when the values of E[$\alpha$] seem to converge, the coefficient $\alpha$ for fully aligned and partially elevation-aligned conditions is still larger than for the other conditions. This is one additional evidence of the alignment condition degrading more the received signal. Please notice that the curves for all the conditions have a similar behavior for $S_4 \geq 0.9$, showing a sudden decrease of E[$\alpha$] as the value of $S_4$ increases. This behavior is similar to that reported in [38].

Based on the relation of (4) with E[$\alpha$], $S_4$, and $\mu$, one can use (3) to estimate the probability of a fading event deeper than a certain threshold (i.e., the CDF). Panels (d), (e), and (f) of Fig. 9 present the estimated probability of having fading events deeper than −15 dB based on (3). This $F_R(-15\text{ dB})$ has been chosen because, according to [39], fading events deeper than −15 dB are likely to cause cycle slips in the receiver tracking loops. As an example, considering the threshold of −15 dB, under strong scintillation cases ($S_4 = 0.9$), for the Presidente Prudente station, the ratios between the probabilities of fading events under fully aligned and partially elevation-aligned, partially azimuth-aligned, and nonaligned cases are 1.22, 1.64 and 1.73,

**TABLE 2.** Average values of $\alpha$ with the respective cumulative density function estimative [%] considering different propagation orientation.

| Site | | Presidente Prudente | | | | São José dos Campos | | | | Porto Alegre | | | |
|---|---|---|---|---|---|---|---|---|---|---|---|---|---|
| | | | $R^2$ (dB) | | | | $R^2$ (dB) | | | | $R^2$ (dB) | | |
| $S_4$ | | E[$\alpha$] | -10 | -15 | -20 | E[$\alpha$] | -10 | -15 | -20 | E[$\alpha$] | -10 | -15 | -20 |
| 0.5 | Aligned | 3.63 | 0.44 | 0.03 | 0.00 | 3.18 | 0.31 | 0.01 | 0.00 | 2.61 | 0.17 | 0.00 | 0.00 |
| | Partially azimuth | 1.78 | 0.05 | 0.00 | 0.00 | 1.57 | 0.03 | 0.00 | 0.00 | 1.55 | 0.03 | 0.00 | 0.00 |
| | Partially elevation | 2.91 | 0.24 | 0.01 | 0.00 | 2.94 | 0.25 | 0.01 | 0.00 | 2.71 | 0.20 | 0.00 | 0.00 |
| | Nonaligned | 2.18 | 0.10 | 0.00 | 0.00 | 2.37 | 0.13 | 0.00 | 0.00 | 1.89 | 0.06 | 0.00 | 0.00 |
| 0.7 | Aligned | 2.90 | 3.02 | 0.57 | 0.10 | 3.05 | 3.24 | 0.64 | 0.13 | 2.50 | 2.40 | 0.37 | 0.05 |
| | Partially azimuth | 1.77 | 1.32 | 0.10 | 0.00 | 1.57 | 1.06 | 0.06 | 0.00 | 1.87 | 1.46 | 0.13 | 0.01 |
| | Partially elevation | 2.75 | 2.79 | 0.49 | 0.08 | 2.97 | 3.13 | 0.61 | 0.11 | 2.53 | 2.44 | 0.38 | 0.05 |
| | Nonaligned | 2.07 | 1.74 | 0.19 | 0.02 | 2.11 | 1.80 | 0.20 | 0.02 | 1.95 | 1.57 | 0.15 | 0.01 |
| 0.9 | Aligned | 2.10 | 6.68 | 1.79 | 0.47 | 2.34 | 7.55 | 2.27 | 0.67 | 2.23 | 7.14 | 2.04 | 0.57 |
| | Partially azimuth | 1.71 | 5.22 | 1.08 | 0.21 | 1.57 | 4.69 | 0.86 | 0.14 | 1.60 | 4.80 | 0.91 | 0.16 |
| | Partially elevation | 1.92 | 6.02 | 1.45 | 0.34 | 2.33 | 7.51 | 2.25 | 0.66 | 1.79 | 5.53 | 1.22 | 0.25 |
| | Nonaligned | 1.68 | 5.09 | 1.03 | 0.19 | 1.85 | 5.74 | 1.32 | 0.29 | 1.17 | 3.23 | 0.37 | 0.03 |
| 1.1 | Aligned | 1.08 | 7.23 | 1.48 | 0.26 | 1.07 | 7.21 | 1.47 | 0.26 | 1.08 | 7.23 | 1.48 | 0.26 |
| | Partially azimuth | 1.07 | 7.22 | 1.48 | 0.26 | 1.17 | 7.88 | 1.80 | 0.36 | - | - | - | - |
| | Partially elevation | 0.94 | 6.38 | 1.11 | 0.15 | 1.00 | 6.79 | 1.27 | 0.20 | 1.01 | 6.79 | 1.29 | 0.20 |
| | Nonaligned | 0.92 | 6.22 | 1.05 | 0.14 | 0.91 | 6.19 | 1.04 | 0.14 | 0.95 | 6.39 | 1.12 | 0.16 |

**TABLE 3.** Coefficients for polynomial approximation of fading coefficient $\alpha$ from (5).

| Condition | Coefficients | Presidente Prudente | São José dos Campos | Porto Alegre |
|---|---|---|---|---|
| Fully aligned | p1 | 0.3863 | 0.2855 | 0.3146 |
| | q1 | -1.6 | -1.627 | -1.525 |
| | q2 | 0.8904 | 0.8424 | 0.7335 |
| | q3 | -0.05661 | -0.04634 | -0.001624 |
| Partially azimuth | p1 | 0.2531 | 0.23 | 0.09841 |
| | q1 | -1.857 | -1.974 | -1.882 |
| | q2 | 1.122 | 1.261 | 1.11 |
| | q3 | -0.08274 | -0.1244 | -0.1456 |
| Partially elevation | p1 | 0.2958 | 0.2725 | 0.3073 |
| | q1 | -1.566 | -1.667 | -1.605 |
| | q2 | 0.8303 | 0.9015 | 0.8934 |
| | q3 | -0.05003 | -0.06539 | -0.06753 |
| Nonaligned | p1 | 0.2605 | 0.3004 | 0.2629 |
| | q1 | -1.743 | -1.688 | -1.9 |
| | q2 | 1.031 | 0.9796 | 1.271 |
| | q3 | -0.08641 | -0.06551 | -0.1579 |

respectively. These results, therefore, show that these deep fading events are 22%, 64% and 73% more likely to occur over Presidente Prudente under fully aligned conditions. Indeed, these results complement the analysis presented by [25] on the rate of deep fading events (<−15 dB) considering the aligned cases for those sites. While this study focuses solely on signals at the GPS-L1 wavelength, it is important to note that in [15], the magnitude of this type of fading is significantly higher for GNSS users operating with shorter wavelength signals, such as GPS L2C and L5. Consequently, the specified values mentioned here are expected to have an even more pronounced impact on these users, as discussed also in [38].

Table 2 summarizes the probabilities of fading events deeper than −10 dB, −15 dB and −20 dB. The values are presented in percentages for fully aligned, partially elevation-aligned, partially azimuth-aligned, and nonaligned conditions. As noted in Fig. 9, comparatively larger values of $\alpha$ can be seen for the fully aligned conditions for all the stations, particularly for $S_4 < 1.1$. As an example, more than 7% of the intensity of the received signal will be at values below −10 dB of nominal value.

Since the $\alpha$-$\mu$ can have infinitely many pairs in (4), for purpose of theoretical work and simulations, approximations will be provided based on the function

$$\widehat{\alpha} = \frac{p1}{\left({S_4}^3 + q_1{S_4}^2 + q_2 S_4 + q_3\right)}, \tag{5}$$

where the $p_1$, $q_1$, $q_2$, and $q_3$ values are provided in Table 3 for the respective sites and conditions. The obtained R-square values for the polynomial fits are generally satisfactory, with

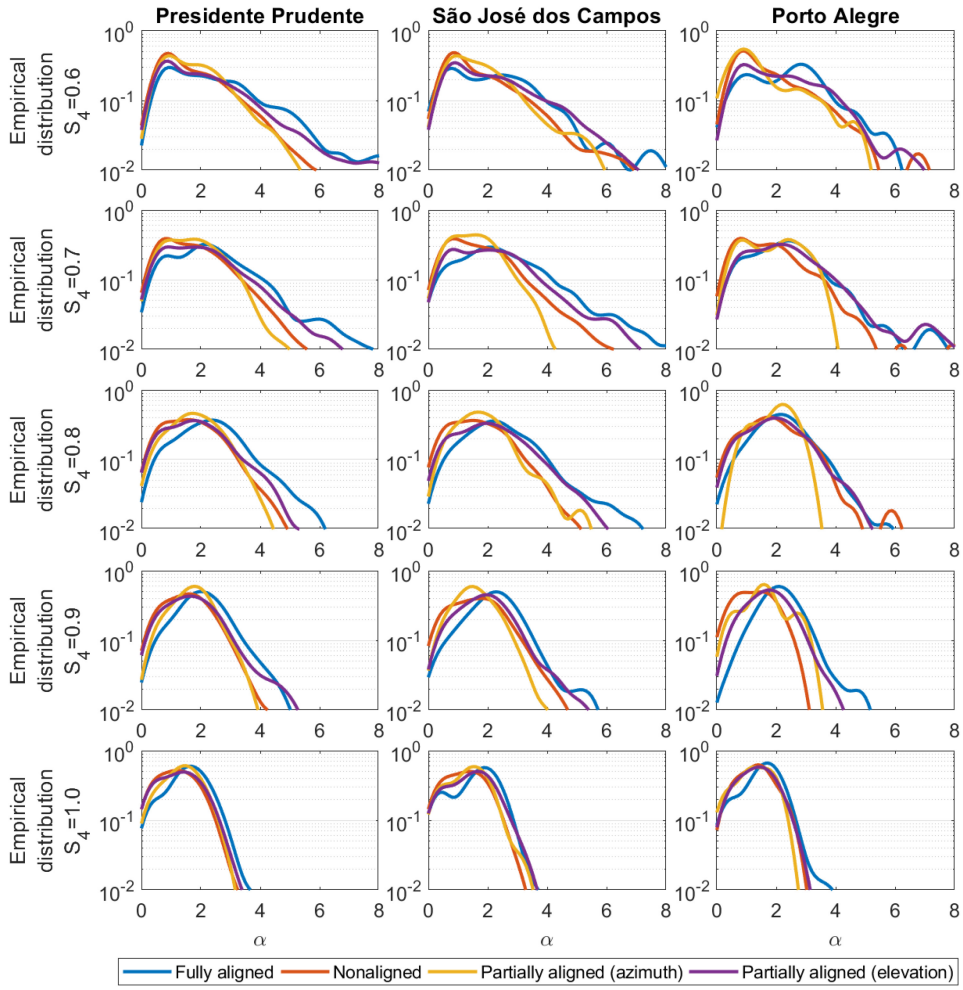


**FIGURE 10.** Distribution functions of $\alpha$ values for Presidente Prudente (left), São José dos Campos (middle) and Porto Alegre (right) considering different $S_4$ ($\pm 0.05$) intervals and the fully aligned, partially elevation-aligned, partially azimuth-aligned and nonaligned conditions.

8 out of 12 values being above 0.97. This indicates that the fitted models explain a significant portion of the variation in the data, providing a good fit. Additionally, the remaining 4 values ranging between 0.82 and 0.93 are considered fair approximations, considering the signal distributions depicted in Figure 10.

Finally, similar to the report of [38], Fig. 10 shows the empirical probability density functions of $\alpha$. The left, middle, and right panels exhibit the results for Presidente Prudente, São José dos Campos, and Porto Alegre, respectively. From the upper down to the lower panels, the values of $S_4$ considered increase from 0.6 up to 1.0. The blue, purple, yellow, and orange lines correspond to fully aligned, partially elevation-aligned, partially azimuth-aligned, and nonaligned conditions, respectively.

It can be noted that the distributions are not symmetrical around their maxima. As the $S_4$ increases it is clear that the distributions become narrower. The fully aligned conditions exhibit the largest spread on the distributions, registering larger values of $\alpha$. These are the most critical cases that may result in the highest occurrence of fading events and, consequently, loss of lock in the GNSS receiver. For example, for $S_4 = 0.9$, in Presidente Prudente and São José dos Campos, the probability of an event with $\alpha = 4$ (extreme severe scintillation) is 10 higher in the fully aligned case than in the nonaligned and partially azimuth-aligned conditions. These results confirm the role of geometry of propagation in the severity of scintillation, with the fully aligned case being the most unfavorable condition for receiving GNSS signals.

## VII. CONCLUDING REMARKS

This paper presents an evaluation of the role of signal propagation orientation relative to geomagnetic field lines and, consequently, to the EPBs, on the statistical scintillation profile of GNSS signals. Data were recorded between November 01, 2014, and March 31, 2015, during the maximum of the solar cycle 24. The hours covered by the dataset are from 19:00 LT up to 23:59 LT. The investigation was carried out using records from three stations in the Brazilian territory, Presidente Prudente, located below the EIA peak, São José dos Campos, located a little south of the EIA peak, and Porto Alegre, located close to the EIA external border. The aspects analyzed were the rate of scintillation and the

fading profile of scintillation. The results obtained in this work suggest a high relevance of the alignment condition in the enhancement of scintillation severity. The main findings and conclusions are presented below.

The complementary cumulative distributions functions indicate that the fully aligned condition presents the highest probabilities of scintillation occurrence in all stations analyzed. The results present abrupt variation from $S_4 = 0.3$ up to $S_4 = 0.7$, suggesting that the fully aligned condition is mostly associated with $S_4 > 0.7$ scenarios.

For the cases of strong scintillation ($S_4 > 0.8$), it was found that the statistic of the fully aligned condition is around 10 times greater than in the partially azimuth-aligned and nonaligned conditions. The fully aligned cases start to contribute to the total number of cases as $S_4$ increases. Partially elevation-aligned condition also has relevant statistics compared to the partially azimuth-aligned and nonaligned cases. The nonaligned condition and partially azimuth-aligned are more coincident with weak and moderate scintillation cases.

Presidente Prudente exhibited less influence of the fully aligned condition. However, as stations more southward are considered, the alignment condition increases its significance. Over Porto Alegre, the alignment condition corresponded to more than 50% of the cases of strong scintillation.

The comparison of the distribution of scintillation according to the difference between the elevation of propagation path and the geomagnetic inclination ($\omega$) and azimuth and the geomagnetic declination ($\nu$) revealed that as $S_4$ increases, the cases become more concentrated around 0°, corresponding to the cases of propagation path aligned in both planes.

The $\alpha$-$\mu$ model showed that the fully aligned cases present stronger amplitude scintillation distribution followed by the partially aligned-elevation. This was found due to the larger $\alpha$ parameter, which implies a more raised tail, meaning higher probability of deep fades. The nonaligned and partially azimuth-aligned cases were those with the smallest values of $\alpha$.

Intensity fading with values of $-15$ dB or below from nominal received signal are, respectively, up to 64% and 73% more likely to occur under the fully aligned and partially elevation-aligned conditions when compared to the nonaligned condition.

The analysis of the distribution of the fading $\alpha$ coefficient showed that fully aligned and partially elevation-aligned conditions are up to 10 times more likely to have elevated $\alpha$ values. This result confirms that the GNSS propagation path aligned with the EPB is a less favorable condition for signal reception, increasing considerably the occurrence of fading events as confirming previous results from the literature in [24] and [25].

These findings reinforce that the propagation path across the EPBs has a great influence on the rate of occurrence of scintillation and on the strength of the fading events in the received signal. Therefore, the propagation orientation of GNSS radio signals in relation to the EPBs plays an important role in affecting the quality of the received signal.

## ACKNOWLEDGMENT

The scintillation monitoring stations deployed in the context of Projects CIGALA/CALIBRA were funded by the European Commission (EC) in the framework of awards FP7-GALILEO-2009-GSA and FP7–GALILEO–2011–GSA–1a, as well of FAPESP award 06/04008-2 and the data was accessed at http://ismrquerytool.fct.unesp.br/is/ using ISMR Query Tools.

## REFERENCES

[1] R. F. Woodman and C. La Hoz, "Radar observations of F region equatorial irregularities," *J. Geophys. Res.*, vol. 81, no. 31, pp. 5447–5466, 1976, doi: 10.1029/JA081i031p05447.

[2] P. M. Kintner, H. Kil, T. L. Beach, and E. R. de Paula, "Fading timescales associated with GPS signals and potential consequences," *Radio Sci.*, vol. 36, no. 4, pp. 731–743, 2001.

[3] K. C. Yeh and C.-H. Liu, "Radio wave scintillations in the ionosphere," *Proc. IEEE*, vol. 70, no. 4, pp. 324–360, Apr. 1982, doi: 10.1109/PROC.1982.12313.

[4] G. Haerendel, J. V. Eccles, and S. Çakir, "Theory for modeling the equatorial evening ionosphere and the origin of the shear in the horizontal plasma flow," *J. Geophys. Res. Space Phys.*, vol. 97, no. A2, pp. 1209–1223, 1992, doi: 10.1029/91JA02226.

[5] S. Basu, E. MacKenzie, and S. Basu, "Ionospheric constraints on VHF/UHF communications links during solar maximum and minimum periods," *Radio Sci.*, vol. 23, no. 3, pp. 363–378, 1988, doi: 10.1029/RS023i003p00363.

[6] L. Marini-Pereira, S. Pullen, A. O. Moraes, and J. Sousasantos, "Ground-based augmentation systems operation in low latitudes—Part 1: Challenges, mitigations, and future prospects," *J. Aerosp. Technol. Manage.*, vol. 13, Dec. 2021, Art. no. e462, doi: 10.1590/jatm.v13.1236.

[7] J. Sousasantos, L. Marini-Pereira, A. O. Moraes, and S. Pullen, "Ground-based augmentation system operation in low latitudes—Part 2: Space weather, ionospheric behavior and challenges," *J. Aerosp. Technol. Manage.*, vol. 13, Oct. 2021, Art. no. e4821, doi: 10.1590/jatm.v13.1237.

[8] C. Rino, *The Theory of Scintillation With Applications in Remote Sensing*. Hoboken, NJ, USA: Wiley, 2011.

[9] M. T. Muella et al., "Climatology and modeling of ionospheric scintillations and irregularity zonal drifts at the equatorial anomaly crest region," *Annales Geophysicae*, vol. 35, no. 6, pp. 1201–1218, Nov. 2017.

[10] J. Sousasantos, A. O. Moraes, J. H. Sobral, M. T. Muella, E. R. de Paula, and R. S. Paolini, "Climatology of the scintillation onset over southern Brazil," *Annales Geophysicae*, vol. 36, no. 2, pp. 565–576, Apr. 2018.

[11] R. P. Silva, J. R. Souza, J. H. A. Sobral, C. M. Denardini, G. L. Borba, and M. A. F. Santos, "Ionospheric plasma bubble zonal drift derived from total electron content measurements," *Radio Sci.*, vol. 54, no. 7, pp. 580–589, 2019, doi: 10.1029/2018RS006727.

[12] A. L. A. Silva, J. Sousasantos, L. Marini-Pereira, L. F. D. Lourenço, A. O. Moraes, and M. A. Abdu, "Evaluation of the dusk and early nighttime total electron content modeling over the eastern Brazilian region during a solar maximum period," *Adv. Space Res.*, vol. 67, no. 5, pp. 1580–1598, 2021, doi: 10.1016/j.asr.2020.12.015.

[13] B. C. Vani et al., "Monitoring ionospheric scintillations with GNSS in South America: Scope, results, and challenges," in *GPS and GNSS Technology in Geosciences*. Amsterdam, The Netherlands: Elsevier, 2021, ch. 13, pp. 255–280, doi: 10.1016/B978-0-12-818617-6.00012-3.

[14] L. A. Salles, B. C. Vani, A. O. Moraes, E. Costa, and E. R. de Paula, "Investigating ionospheric scintillation effects on multifrequency GPS signals," *Surveys Geophys.*, vol. 42, no. 4, pp. 999–1025, 2021, doi: 10.1007/s10712-021-09643-7.

[15] L. A. Salles, A. O. Moraes, B. C. Vani, J. Sousasantos, B. J. Affonso, and J. F. G. Monico, "A deep fading assessment of the modernized L2C and L5 signals for low-latitude regions," *GPS Solut.*, vol. 25, no. 3, p. 112, 2021, doi: 10.1007/s10291-021-01157-4.

[16] P. M. Kintner, B. M. Ledvina, E. R. de Paula, and I. J. Kantor, "Size, shape, orientation, speed, and duration of GPS equatorial anomaly scintillations," *Radio Sci.*, vol. 39, no. 2, pp. 1–23, 2004, doi: 10.1029/2003RS002878.

[17] A. O. Akala, P. H. Doherty, C. S. Carrano, C. E. Valladares, and K. M. Groves, "Impacts of ionospheric scintillations on GPS receivers intended for equatorial aviation applications," *Radio Sci.*, vol. 47, no. 4, pp. 1–11, 2012, doi: 10.1029/2012RS004995.

[18] S. Priyadarshi and A. W. Wernik, "Variation of the ionospheric scintillation index with elevation angle of the transmitter," *Acta Geophysica*, vol. 61, no. 5, pp. 1279–1288, 2013, doi: 10.2478/s11600-013-0123-3.

[19] Y. Liu and S. Radicella, "On the correlation between ROTI and S4," *Annales Geophysicae Discuss.*, pp. 1–14, 2019, doi: 10.5194/angeo-2019-147.

[20] S. Goswami, S. Ray, and A. Paul, "Degradation of satellite-based navigation performance observed from an anomaly crest location in the Indian longitude sector," *Radio Sci.*, vol. 55, no. 8, pp. 1–16, 2020, doi: 10.1029/2019RS007042.

[21] A. DasGupta, S. Ray, A. Paul, P. Banerjee, and A. Bose, "Errors in position-fixing by GPS in an environment of strong equatorial scintillations in the Indian zone," *Radio Sci.*, vol. 39, no. 1, pp. 1–8, 2004, doi: 10.1029/2002RS002822.

[22] B. J. Affonso, A. Moraes, J. Sousasantos, L. Marini-Pereira, and S. Pullen, "Strong ionospheric spatial gradient events induced by signal propagation paths aligned with equatorial plasma bubbles," *IEEE Trans. Aerosp. Electron. Syst.*, vol. 58, no. 4, pp. 2868–2879, Aug. 2022.

[23] A. O. Moraes et al., "The variability of low-latitude ionospheric amplitude and phase scintillation detected by a triple-frequency GPS receiver," *Radio Sci.*, vol. 52, no. 4, pp. 439–460, 2017, doi: 10.1002/2016RS006165.

[24] A. O. Moraes et al., "GPS availability and positioning issues when the signal paths are aligned with ionospheric plasma bubbles," *GPS Solut.*, vol. 22, no. 4, p. 95, 2018, doi: 10.1007/s10291-018-0760-8.

[25] J. Sousasantos et al., "Amplitude scintillation severity and fading profiles under alignment between GPS propagation paths and equatorial plasma bubbles," *Space Weather*, vol. 20, no. 11, 2022, Art. no. e2022SW003243, doi: 10.1029/2022SW003243.

[26] M. D. Yacoub, "The $\alpha$-$\mu$ distribution: A physical fading model for the stacy distribution," *IEEE Trans. Veh. Technol.*, vol. 56, no. 1, pp. 27–34, Jan. 2007, doi: 10.1109/TVT.2006.883753.

[27] A. O. Moraes, E. Costa, E. R. de Paula, W. J. Perrella, and J. F. G. Monico, "Extended ionospheric amplitude scintillation model for GPS receivers," *Radio Sci.*, vol. 49, no. 5, pp. 315–329, 2014, doi: 10.1002/2013RS005307.

[28] E. Thébault et al., "Evaluation of candidate geomagnetic field models for IGRF-12," *Earth, Planets and Space*, vol. 67, no. 1, p. 112, 2015, doi: 10.1186/s40623-015-0273-4.

[29] J. F. G. Monico et al., "The GNSS NavAer INCT project overview and main results," *J. Aerosp. Technol. Manage.*, vol. 14, Jan. 2022, Art. no. e0722, doi: 10.1590/jatm.v14.1249.

[30] E. R. de Paula et al., "Performance of 6 different global navigation satellite system receivers at low latitude under moderate and strong scintillation," *Earth Space Sci.*, vol. 8, no. 2, 2021, Art. no. e2020EA001314, doi: 10.1029/2020EA001314.

[31] E. J. Fremouw et al., "Early results from the DNA wideband satellite experiment—Complex-signal scintillation," *Radio Sci.*, vol. 13, no. 1, pp. 167–187, 1978.

[32] T. E. Humphreys, M. L. Psiaki, and P. M. Kintner, "Modeling the effects of ionospheric scintillation on GPS carrier phase tracking," *IEEE Trans. Aerosp. Electron. Syst.*, vol. 46, no. 4, pp. 1624–1637, Oct. 2010, doi: 10.1109/TAES.2010.5595583.

[33] A. O. Moraes, E. R. de Paula, W. J. Perrella, and F. da Silveira Rodrigues, "On the distribution of GPS signal amplitudes during low-latitude ionospheric scintillation," *GPS Solut.*, vol. 17, no. 4, pp. 499–510, 2012, doi: 10.1007/s10291-012-0295-3.

[34] A. O. Moraes, E. R. de Paula, M. T. de Assis Honorato Muella, and W. J. Perrella, "On the second order statistics for GPS ionospheric scintillation modeling," *Radio Sci.*, vol. 49, no. 2, pp. 94–105, 2014, doi: 10.1002/2013RS005270.

[35] V. E. Gherm and N. N. Zernov, "Strong scintillation of GNSS signals in the inhomogeneous ionosphere: 2. Simulator of transionospheric channel," *Radio Sci.*, vol. 50, no. 2, pp. 168–176, 2015, doi: 10.1002/2014RS005604.

[36] T. M. S. Espejo, E. Costa, A. O. Moraes, A. R. F. Martinon, E. R. de Paula, and J. F. G. Monico, "A GPS signal-in-space simulation model for equatorial and low latitudes in the Brazilian longitude sector," *GPS Solut.*, vol. 26, no. 3, pp. 1–13, 2022, doi: 10.1007/s10291-022-01273-9.

[37] W. N. Venables and B. D. Ripley, *Modern Applied Statistics With S-PLUS*. New York, NY, USA: Springer, 2013, doi: 10.1007/978-1-4757-3121-7.

[38] A. O. Moraes et al., "Ionospheric scintillation fading coefficients for the GPS L1, L2, and L5 frequencies," *Radio Sci.*, vol. 53, no. 9, pp. 1165–1174, 2018, doi: 10.1029/2018RS006653.

[39] I. P. Portella, A. O. Moraes, M. da Silva Pinho, J. Sousasantos, and F. Rodrigues, "Examining the tolerance of GNSS receiver phase tracking loop under the effects of severe ionospheric scintillation conditions based on its bandwidth," *Radio Sci.*, vol. 56, no. 6, pp. 1–11, 2021, doi: 10.1029/2020RS007160.

[40] L. Marini-Pereira, L. F. D. Lourenço, J. Sousasantos, A. O. Moraes, and S. Pullen, "Regional ionospheric delay mapping for low-latitude environments," *Radio Sci.*, vol. 55, no. 12, pp. 1–16, 2020.